



HAL
open science

Exploring the thermoelectric behavior of spark plasma sintered Fe_{7-x}Co_xS₈ compounds

Juliette Simon, Gabin Guelou, Bhuvanesh Srinivasan, David Berthebaud, Takao Mori, Antoine Maignan

► To cite this version:

Juliette Simon, Gabin Guelou, Bhuvanesh Srinivasan, David Berthebaud, Takao Mori, et al.. Exploring the thermoelectric behavior of spark plasma sintered Fe_{7-x}Co_xS₈ compounds. *Journal of Alloys and Compounds*, 2020, 819, pp.152999. 10.1016/j.jallcom.2019.152999 . hal-02991415

HAL Id: hal-02991415

<https://hal.science/hal-02991415>

Submitted on 9 Nov 2020

HAL is a multi-disciplinary open access archive for the deposit and dissemination of scientific research documents, whether they are published or not. The documents may come from teaching and research institutions in France or abroad, or from public or private research centers.

L'archive ouverte pluridisciplinaire **HAL**, est destinée au dépôt et à la diffusion de documents scientifiques de niveau recherche, publiés ou non, émanant des établissements d'enseignement et de recherche français ou étrangers, des laboratoires publics ou privés.

Exploring the thermoelectric behavior of Spark Plasma Sintered $\text{Fe}_{7-x}\text{Co}_x\text{S}_8$ compounds

Juliette Simon¹, Gabin Guélou¹, Bhuvanesh Srinivasan^{1,2}, David Berthebaud^{2,3*}, Takao Mori^{1,4} and Antoine Maignan^{3*}

1. WPI International Center for Materials Nanoarchitectonics (WPI-MANA) and Center for Functional Sensor & Actuator (CFSN), National Institute for Materials Science (NIMS), Namiki 1-1, Tsukuba 305-0044, Japan

2. CNRS-Saint Gobain-NIMS, UMI 3629, Laboratory for Innovative Key Materials and Structures (LINK), National Institute for Materials Science, Tsukuba 305-0044, Japan

3. Laboratoire CRISMAT, Normandie Univ., ENSICAEN, UNICAEN, CNRS, 14000 Caen, France

4. Graduate School of Pure and Applied Sciences, University of Tsukuba, Tsukuba 305-8671, Japan

* Correspondences: David.BERTHEBAUD@cnrs.fr; antoine.maignan@ensicaen.fr

Abstract

Sulfide-based materials are emerging as viable alternatives for the current state-of-the-art thermoelectric materials, which usually are composed of toxic, expensive and scarce elements. Here, a systematic study of one such inexpensive and environmentally friendly sulfide-based system, *i.e.* $\text{Fe}_{7-x}\text{Co}_x\text{S}_8$ pyrrhotite-type compounds that were synthesized by solid-state reaction and densified by Spark Plasma Sintering are investigated for their structural and thermoelectric properties. We report that substitution of Co for Fe in pyrrhotites: (i) induces structural transition from monoclinic 4C superstructure to trigonal 3C superstructure; (ii) modifies the magnetic behavior by decreasing the magnetic ordering temperature and magnetization; (iii) alters the type of dominant charge carriers (from *p*- to *n*-type) and enhances their electrical transport properties; (iv) mitigates the phonon contribution to the thermal conductivity; and (v) amplifies the thermoelectric figure of merit when compared with that of pristine pyrrhotites.

Keywords: Co-doped Pyrrhotites; Sulfides; SPS; Thermoelectrics; Structural transition; Improved power factor

1. Introduction

Thermoelectric (TE) materials and devices have drawn increasing interest and attention due to their potential to reversibly convert waste heat into electricity [1–4]. The TE material's efficiency is quantified by a dimensionless figure of merit, $zT = S^2\sigma T/\kappa$ where S , σ , T and κ are the Seebeck coefficient, electrical conductivity, absolute temperature and total thermal conductivity (sum of the electronic part, κ_e , and the lattice part, κ_{lat}), respectively. Industrial applications require large-scale economic and environmentally benign high performance TE materials. However, the current state-of-the-art TE materials are usually composed of expensive, scarce, or toxic heavy elements such as Pb, Te, Bi, Ge, Sb

etc [5–12]. In the past few years, sulfide materials have gained considerable limelight due to their wide range of potential applications ranging from photovoltaics to thermoelectrics [13]. Among those sulfide materials, particular attention has been given to copper-based compounds such as Cu_{2-x}S , chalcopyrites, cubanites, colusites and high-entropy copper sulfides [14–18]. However, not much information is available on the Cu-free sulfides for TE application. In this work, one such Cu-free sulfide is explored, *i.e.* pyrrhotite-type Fe_7S_8 compounds have been looked at, as both Fe and S are inexpensive, non-toxic and are more abundant in earth's crust. The cobalt substitution for iron, *i.e.* bringing more electrons, is also investigated in this present work. The choice of this material system also stems from their interesting superstructure formations and magnetic structural transitions [19,20], which could play a role in their electrical and thermal transport properties. Magnetic enhancement of TE properties has previously been reported in some systems [21,22]. Although magnetic and structural properties of these pyrrhotite compounds have been widely studied, their TE behavior has never been explored, especially on the cobalt-doped pyrrhotites, which this work aims to shed some light on.

2. Materials & Methods

The samples of $\text{Fe}_{7-x}\text{Co}_x\text{S}_8$ ($0 \leq x \leq 7$) were prepared by a two-step process: firstly, the ingots were obtained by the vacuum sealed-tube melting process (heated at 1223 K for 24 h), and secondly, the obtained ingots were crushed into powders and consolidated by Spark Plasma Sintering (SPS-1080 – SPS Syntex Inc.) at 773 K (heating rate ~ 60 K/min) for 15 mins (holding time) under an axial pressure of 75 MPa in Ar atmosphere. The sintered discs were then cut and polished to the required shapes and dimensions for various thermoelectric measurements.

Powder X-ray diffraction

Powder X-ray diffraction (PXRD) patterns were recorded at room temperature in the 2θ range of $10^\circ - 90^\circ$ in 1 hour using a PANalytical X'Pert Pro diffractometer (Cu $K_{\alpha 1}/K_{\alpha 2}$ radiation, $\lambda = 1.540598 \text{ \AA}$, 1.544426 \AA , PIXcel 1D detector). Le bail fitting was performed using FullProf program [23] included in the WinPLOTR software.

Electrical and thermal transport measurements

The electrical resistivity and Seebeck coefficient were measured simultaneously using a commercial instrument (ZEM-2, ADVANCE RIKO Inc.) under the partial pressure of He on $\sim 2 \times 2 \times 6 \text{ mm}^3$ bars.

The temperature dependent thermal diffusivity, D , was measured using the laser flash diffusivity method in LFA-467 Hyperflash (Netzsch) on disk-shaped samples of 10 mm diameter and ~ 2 mm thickness. The temperature dependent heat capacity, C_p , was derived using a standard sample (pyroceram) in LFA-467, which is in good agreement with the Dulong–Petit C_p value. The total thermal conductivity was calculated using the formula, $\kappa = DC_p\rho$, where ρ is the density of the sample (measured using Archimedes' principle). To better understand the thermal transport properties, the contributions from electronic and lattice parts were calculated. The lattice thermal conductivity (κ_{lat}) was estimated from κ by subtracting the electronic contribution (κ_e) via Wiedemann-Franz law, as in the following equation,

$$\kappa_e = L\sigma T$$

where κ_e is the electronic thermal conductivity and L is the Lorenz number computed by the condensed version of Single Parabolic Band model with acoustic phonon scattering (SPB-APS), as in the following equation,

$$L = 1.5 + \exp \left[-\frac{|S|}{116} \right]$$

where Seebeck coefficient (S) is in μVK^{-1} and Lorenz number (L) is in $10^{-8} \text{W}\Omega\text{K}^{-2}$.

The uncertainty in the results for the values of electrical and thermal transport properties was $\sim 5\%$ and $\sim 7\%$, respectively and for the overall zT was $\sim 12\%$. Error bars are not shown in the figures to increase readability.

Differential scanning calorimetry (DSC) analysis was performed using Thermo-plus EVO (Rigaku Co.) on a small piece of the bulk sample ($\sim 30 \text{ mg}$).

Magnetic measurements

The magnetization, M was measured as a function of temperature, T (at a constant $H = 100 \text{ Oe}$) and as a function of external field, H (at a constant $T = 2.5 \text{ K}$) using the Magnetic Properties Measurement System (MPMS, Quantum Design). ZFC mode during heating cycle ($4 \text{ K} - 300 \text{ K}$) and FCC mode during cooling cycle ($300 \text{ K} - 4 \text{ K}$). A small piece of the sample ($\sim 20 \text{ mg}$) was loaded into a gelatin capsule for the magnetic measurements.

3. Results and discussion

Highly densified samples of $\text{Fe}_{7-x}\text{Co}_x\text{S}_8$ ($x = 0, 2.8, 4.2, 5, 6, 6.5, 7$) were obtained after SPS processing. The density of the sintered disks was found to be $\sim 97\%$ of the theoretical density. It must be noted that it is a unique highlight from this work, as such compounds have never been processed by SPS in the past. So far, such Fe_7S_8 based pyrrhotite-type compounds that were presented in the literature were usually synthesized by the conventional (one-step process) sealed-tube melting route [19,20]. The rationale for employing this 2-step process *via* SPS is that, it has been proved time and again that SPS processing can control the grain growth [24] and can induce nanoscale defects and precipitates, thus scattering a wide spectrum of heat carrying phonons (panoscopic approach [25,26]) when compared to the conventional melt processing (one-step process) route [7,27–29]. Importantly, PXRD pattern did not show evidence of any structural change after SPS processing (Supporting Info – SI, Figure S1). Only peak sharpness was slightly increased due to an increased crystallinity through SPS processing. Similar to the work of Baranov *et al.* [20], our pristine Fe_7S_8 compound was found to crystallize in the monoclinic 4C superstructure (space group $C2/c$) with parameters $a = 11.931(3) \text{ \AA}$, $b = 6.886(6) \text{ \AA}$, $c = 12.891(1) \text{ \AA}$ and $\beta = 117.20(1)^\circ$. Cobalt substituted samples were found to crystallize in the trigonal 3C superstructure (space group $P3_121$, SI, Figure S2). In the $\text{Fe}_{7-x}\text{Co}_x\text{S}_8$ series, for the values of $x > 5$, secondary phases that could not be indexed with the existing databases were present. Hence, in the forthcoming sections of this paper, the discussion is limited to the solubility or solid-solution limit ($x \leq 5$). Our results show that the Co for Fe substitution in the $\text{Fe}_{7-x}\text{Co}_x\text{S}_8$ system leads to changes in the crystal structure with the formation of a different NiAs superstructure. According to Baranov *et al.* [20], such $\text{Fe}_{7-x}\text{Co}_x\text{S}_8$ compounds have a layered crystal structure of the NiAs-type and can be characterized by the lattice parameters a_0 and c_0 of the primitive NiAs-type unit cell. The evolution of the calculated lattice parameters a_0 and c_0 is presented in Figure 1. The decreasing trend of c_0 stipulates at the decrease of the inter-layer distances with the substitution of Co for Fe. In other words, addition of Co leads to the contraction of the crystal lattice, which is in agreement with the previous reports [20,30]. The a_0 parameter is rather constant with Co substitution (contrary to the c_0 parameter), implicating a substantially different compressibility of the crystal lattice perpendicular and parallel to the layers.

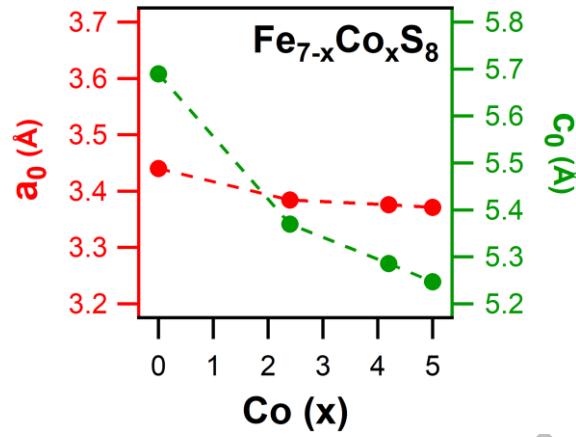


Figure 1. Lattice parameters a_0 and c_0 as function of cobalt content in the $\text{Fe}_{7-x}\text{Co}_x\text{S}_8$ ($0 \leq x \leq 5$) series.

Interestingly, the cobalt substitution enhances the electrical conductivity by about 2 orders of magnitude (Figure 2a) when compared to that of pristine pyrrhotite. Moreover, substitution of Fe by Co induces a sign change of the room temperature Seebeck coefficient from positive to negative (Figure 2b). This suggests that the transport turns from p -type in pristine sample to n -type as cobalt adds electrons in the pyrrhotite. Even in this pristine pyrrhotite, the n -type charge carriers begin to dominate the transport at temperatures above 525 K, which is discussed based on their electronic band structure in the following section. Both the increase in the electrical conductivity and the modification in Seebeck behavior (p - to n -type) with cobalt substitution can be attributed to the increase of the charge carrier concentration as the electrons begin to fill the conduction band when Co is substituted for Fe. The cation Co^{2+} has one more electron in its valence shell than Fe^{2+} . Due to the changes in σ and S , the thermoelectric power factor ($PF = S^2\sigma$) is significantly improved with cobalt substitution (Figure 2c). The σ increase with cobalt substitution impacts the total thermal conductivity (Figure 2d), mainly through the higher contribution from the electronic part, κ_e (SI, Figure S3(c)). More interestingly, it must be noted that the lattice part of the thermal conductivity, κ_{lat} is also significantly reduced with the Co substitution (Figure 2e), possibly due to reasons such as local defects (segregation of 3C defects in the 4C), role of magnons, and micro/nano-scale artifacts formed during the SPS processing. The cumulative effect of noted improvement in the electrical transport and a considerable suppression of the thermal transport (phonon) with cobalt doping is obviously enhancing the zT (Figure 2f). The Co substituted sample with the composition of $x = 0.05$ exhibited the highest $zT \sim 0.004$ at 573 K, which is few orders of magnitude greater than that of related pristine pyrite that was reported very recently [31]. However, it must be noted that these zT values are too low for any potential industrial application.

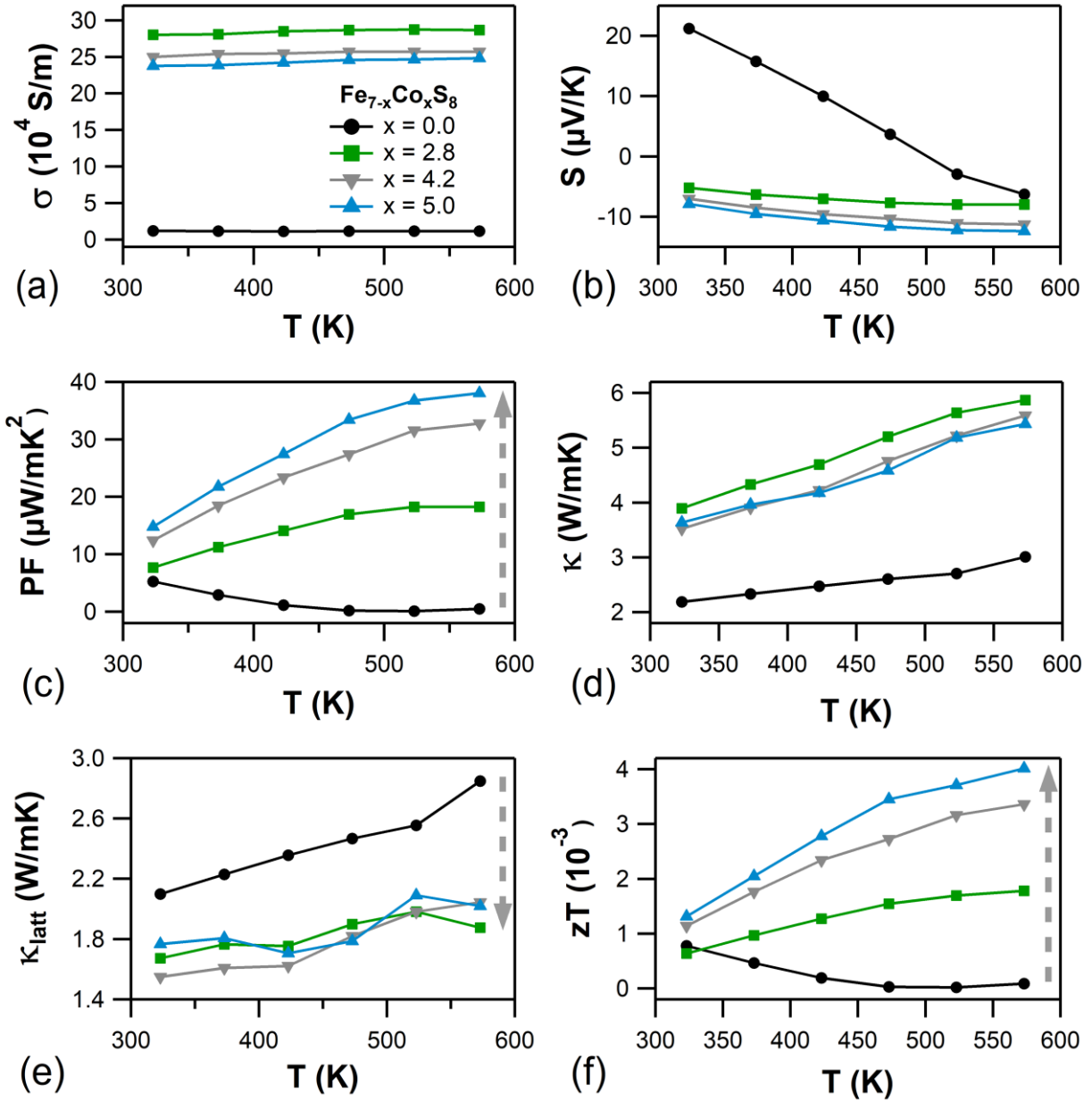


Figure 2. Temperature dependent transport properties for $\text{Fe}_{7-x}\text{Co}_x\text{S}_8$ series ($0 \leq x \leq 5$) – (a) electrical conductivity, σ , (b) Seebeck coefficient, S , (c) Power factor, PF , (d) Total thermal conductivity, κ , (e) Lattice thermal conductivity, κ_{latt} , and (f) figure of merit, zT . The uncertainty in the results for the values of electrical and thermal transport properties was $\sim 5\%$ and $\sim 7\%$, respectively and for the overall zT was $\sim 12\%$. Error bars are not shown in the figures to increase readability.

The temperature dependent specific heat (C_p) data obtained from the differential scanning calorimetry (DSC) analysis evidences some potential structural transition happening in the pristine pyrrhotite at ~ 590 K (Figure 3). Based on their magnetic measurements, Powell *et al.* [19] suggested a phase transition from monoclinic 4C magnetically ordered state to a hexagonal NiAs cation deficient state (1C) at 598 K for the pristine Fe_7S_8 . The sharp bump at ~ 590 K from our DSC data for the pristine sample supports their phase transition (from 4C to 1C) claim, which was based on their magnetic measurement data. In the ferrimagnetic state (below $T_C \approx 600\text{K}$), the electronic band structure of Fe_7S_8 differs considerably from that of the paramagnetic state owing to the large exchange splitting (~ 3.2 eV) of the 3d states of

each Fe-site, and in the non-magnetic state, the Fermi level lies at the higher energy side of the electronic density of states in the non-bonding part of the hybridized bands composed of Fe 3*d* and S 3*p* orbitals [32]. This explains the *p*- to *n*-type transport change with temperature for the pristine pyrrhotite. From C_p , no such phase transition (in relation with the 3C structural ordering) was observed for the cobalt doped samples in this measurement range from 323 K to 673 K.

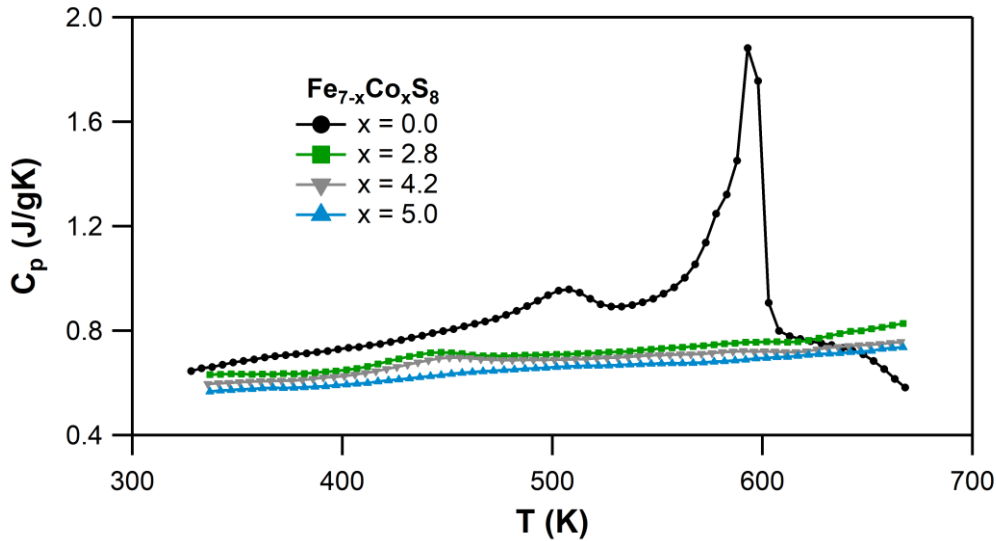


Figure 3. Temperature dependent specific heat, C_p obtained from DSC analysis for $\text{Fe}_{7-x}\text{Co}_x\text{S}_8$ ($0 \leq x \leq 5$) compounds.

The substitution of Co for Fe reduced the magnetization, as can be referred from Figure 4a, which displays the M versus H dependences on the $\text{Fe}_{7-x}\text{Co}_x\text{S}_8$ ($0 \leq x \leq 5$) compounds at $T = 2.5$ K. The magnetic ordering temperature was also observed to decrease with Co content, as can be referred from the temperature dependences of the magnetization measured at $H = 100$ Oe (Figure 4b). The magnetic behavior of these compounds is found to be consistent with the previously reported work [20], despite the differences in their synthesis methodology. Magnetic enhancement has been reported for some systems [21,22], however, in this case, the improvement in the thermoelectric properties appear to be driven by the changes in the charge carriers.

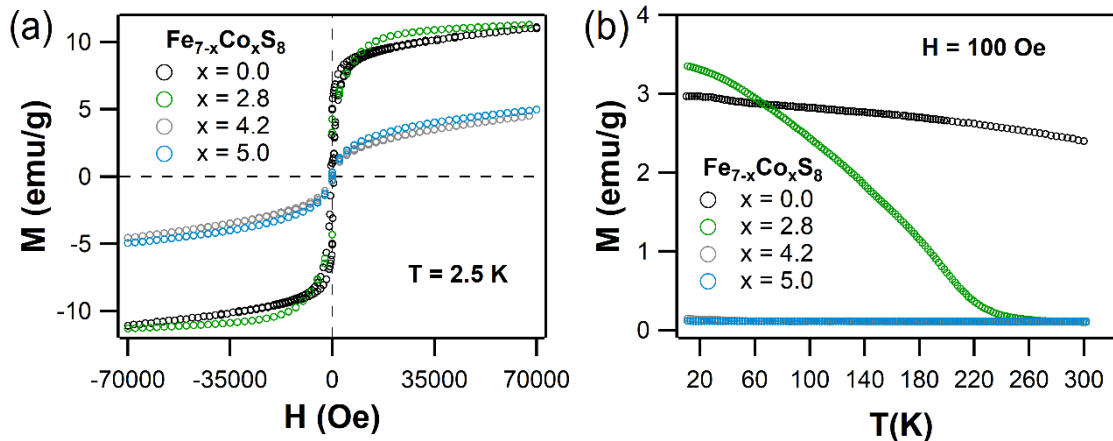


Figure 4. Magnetic behavior of $\text{Fe}_{7-x}\text{Co}_x\text{S}_8$ ($0 \leq x \leq 5$) compounds – (a) field dependences of the magnetization measured at $T = 2.5$ K, (b) temperature dependences of the magnetization measured at a fixed magnetic field of 100 Oe.

4. Conclusion

Highly dense samples of $\text{Fe}_{7-x}\text{Co}_x\text{S}_8$ ($0 \leq x \leq 5$) compounds were successfully synthesized by a two-step process (melt-processing followed by SPS). Substitution of Co for Fe in pyrrhotites was found to induce some following changes: (i) modification of the crystal structure and to the formation of different superstructure derived from NiAs (from monoclinic 4C to trigonal 3C); (ii) increasing the charge carrier density, and altering the type of majority charge carriers from *p*- to *n*-type, thus resulting in a notable enhancement in the electrical transport (*i.e.*, improved thermoelectric power factor); (iii) considerable suppression of the phonon contribution to the thermal conductivity; (iv) significant boost in the thermoelectric figure of merit (albeit not much significant for a practical application); and (v) reduction in their magnetic ordering temperature and the magnetization. In addition, the pristine Fe_7S_8 compound was found to undergo a phase transition from monoclinic 4C magnetically ordered state to a hexagonal NiAs cation deficient state at ~ 590 K, which fits to the T_C values reported for that iron sulfide. This outlines the strong interplay between structure, magnetism and electronic transport in the $\text{Fe}_{7-x}\text{Co}_x\text{S}_8$ compounds.

Acknowledgement

B.S, T.M thank JSPS postdoctoral Fellowship P19720, KAKENHI 19F19720, JST CREST JPMJCR15Q6, JPMJCR19Q.

References

- [1] I. Petsagkourakis, K. Tybrandt, X. Crispin, I. Ohkubo, N. Satoh, T. Mori, Thermoelectric materials and applications for energy harvesting power generation, *Sci. Technol. Adv. Mater.* 19 (2018) 836–862. doi:10.1080/14686996.2018.1530938.
- [2] T.M. Tritt, M.A. Subramanian, Thermoelectric Materials, Phenomena, and Applications: A Bird's Eye View, *MRS Bull.* 31 (2006) 188–198.
- [3] T. Mori, S. Priya, Materials for energy harvesting: At the forefront of a new wave, *MRS Bull.* 43 (2018) 176–180. doi:10.1557/mrs.2018.32.
- [4] B. Srinivasan, S. Cui, C. Prestipino, A. Gellé, C. Boussard-Pledel, S. Ababou-Girard, A. Trapananti, B. Bureau, S. Di Matteo, Possible Mechanism for Hole Conductivity in Cu–As–Te Thermoelectric Glasses: A XANES and EXAFS Study, *J. Phys. Chem. C.* 121 (2017) 14045–14050. doi:10.1021/acs.jpcc.7b04555.
- [5] S. Perumal, S. Roychowdhury, K. Biswas, High performance thermoelectric materials and devices based on GeTe, *J. Mater. Chem. C.* 4 (2016) 7520–7536. doi:10.1039/C6TC02501C.
- [6] B. Srinivasan, C. Boussard-Pledel, V. Dorcet, M. Samanta, K. Biswas, R. Lefèvre, F. Gascoin, F. Cheviré, S. Tricot, M. Reece, B. Bureau, Thermoelectric Properties of Highly-Crystallized Ge–Te–Se Glasses Doped with Cu/Bi, *Materials.* 10 (2017) 328. doi:10.3390/ma10040328.
- [7] K. Biswas, J. He, I.D. Blum, C.-I. Wu, T.P. Hogan, D.N. Seidman, V.P. Dravid, M.G. Kanatzidis, High-performance bulk thermoelectrics with all-scale hierarchical architectures, *Nature.* 489 (2012) 414–418. doi:10.1038/nature11439.

- [8] B. Srinivasan, A. Gellé, J.-F. Halet, C. Boussard-Pledel, B. Bureau, Detrimental Effects of Doping Al and Ba on the Thermoelectric Performance of GeTe, *Materials*. 11 (2018) 2237. doi:10.3390/ma11112237.
- [9] G.J. Snyder, E.S. Toberer, Complex thermoelectric materials, *Nat. Mater.* 7 (2008) 105–114. doi:10.1038/nmat2090.
- [10] B. Srinivasan, R. Gautier, F. Gucci, B. Fontaine, J.-F. Halet, F. Cheviré, C. Boussard-Pledel, M.J. Reece, B. Bureau, Impact of Coinage Metal Insertion on the Thermoelectric Properties of GeTe Solid-State Solutions, *J. Phys. Chem. C*. 122 (2018) 227–235. doi:10.1021/acs.jpcc.7b10839.
- [11] Y. Pei, X. Shi, A. LaLonde, H. Wang, L. Chen, G.J. Snyder, Convergence of electronic bands for high performance bulk thermoelectrics, *Nature*. 473 (2011) 66–69. doi:10.1038/nature09996.
- [12] B. Srinivasan, F. Gucci, C. Boussard-Pledel, F. Cheviré, M.J. Reece, S. Tricot, L. Calvez, B. Bureau, Enhancement in thermoelectric performance of n-type Pb-deficit Pb-Sb-Te alloys, *J. Alloys Compd.* 729 (2017) 198–202. doi:10.1016/j.jallcom.2017.09.135.
- [13] F.-J. Fan, L. Wu, S.-H. Yu, Energetic I–III–VI₂ and I₂–II–IV–VI₄ nanocrystals: synthesis, photovoltaic and thermoelectric applications, *Energy Environ. Sci.* 7 (2013) 190–208. doi:10.1039/C3EE41437J.
- [14] Y. He, T. Day, T. Zhang, H. Liu, X. Shi, L. Chen, G.J. Snyder, High Thermoelectric Performance in Non-Toxic Earth-Abundant Copper Sulfide, *Adv. Mater.* 26 (2014) 3974–3978. doi:10.1002/adma.201400515.
- [15] R. Lefèvre, D. Berthebaud, M.Y. Mychinko, O.I. Lebedev, T. Mori, F. Gascoin, A. Maignan, Thermoelectric properties of the chalcopyrite Cu_{1-x}M_xFeS_{2-y} series (M = Mn, Co, Ni), *RSC Adv.* 6 (2016) 55117–55124. doi:10.1039/C6RA10046E.
- [16] T. Barbier, D. Berthebaud, R. Frésard, O.I. Lebedev, E. Guilmeau, V. Eyert, A. Maignan, Structural and thermoelectric properties of n-type isocubanite CuFe₂S₃, *Inorg. Chem. Front.* 4 (2017) 424–432. doi:10.1039/C6QI00510A.
- [17] C. Bourgès, Y. Bouyrie, A.R. Supka, R. Al Rahal Al Orabi, P. Lemoine, O.I. Lebedev, M. Ohta, K. Suekuni, V. Nassif, V. Hardy, R. Daou, Y. Miyazaki, M. Fornari, E. Guilmeau, High-Performance Thermoelectric Bulk Colusite by Process Controlled Structural Disorder, *J. Am. Chem. Soc.* 140 (2018) 2186–2195. doi:10.1021/jacs.7b11224.
- [18] R.-Z. Zhang, F. Gucci, H. Zhu, K. Chen, M.J. Reece, Data-Driven Design of Ecofriendly Thermoelectric High-Entropy Sulfides, *Inorg. Chem.* 57 (2018) 13027–13033. doi:10.1021/acs.inorgchem.8b02379.
- [19] A.V. Powell, P. Vaquero, K.S. Knight, L.C. Chapon, R.D. Sánchez, Structure and magnetism in synthetic pyrrhotite Fe₇S₈: A powder neutron-diffraction study, *Phys. Rev. B*. 70 (2004) 014415. doi:10.1103/PhysRevB.70.014415.
- [20] N.V. Baranov, P.N.G. Ibrahim, N.V. Selezneva, A.F. Gubkin, A.S. Volegov, D.A. Shishkin, L. Keller, D. Sheptyakov, E.A. Sherstobitova, Layer-preferential substitutions and magnetic properties of pyrrhotite-type Fe_{7-y}M_yX₈ chalcogenides (X = S, Se; M = Ti, Co), *J. Phys. Condens. Matter*. 27 (2015) 286003. doi:10.1088/0953-8984/27/28/286003.
- [21] J.-B. Vaney, S. Aminorroaya Yamini, H. Takaki, K. Kobayashi, N. Kobayashi, T. Mori, Magnetism-mediated thermoelectric performance of the Cr-doped bismuth telluride tetradymite, *Mater. Today Phys.* 9 (2019) 100090. doi:10.1016/j.mtphys.2019.03.004.
- [22] N. Tsujii, A. Nishide, J. Hayakawa, T. Mori, Observation of enhanced thermopower due to spin fluctuation in weak itinerant ferromagnet, *Sci. Adv.* 5 (2019) eaat5935. doi:10.1126/sciadv.aat5935.
- [23] J. Rodríguez-Carvajal, Recent advances in magnetic structure determination by neutron powder diffraction, *Phys. B Condens. Matter*. 192 (1993) 55–69. doi:10.1016/0921-4526(93)90108-I.
- [24] O. Guillon, J. Gonzalez-Julian, B. Dargatz, T. Kessel, G. Schierning, J. Räthel, M. Herrmann, Field-Assisted Sintering Technology/Spark Plasma Sintering: Mechanisms, Materials, and Technology Developments, *Adv. Eng. Mater.* 16 (2014) 830–849. doi:10.1002/adem.201300409.
- [25] L.-D. Zhao, V.P. Dravid, M.G. Kanatzidis, The panoscopic approach to high performance thermoelectrics, *Energy Environ. Sci.* 7 (2013) 251–268. doi:10.1039/C3EE43099E.
- [26] J. He, M.G. Kanatzidis, V.P. Dravid, High performance bulk thermoelectrics via a panoscopic approach, *Mater. Today*. 16 (2013) 166–176. doi:10.1016/j.mattod.2013.05.004.

- [27] B. Srinivasan, B. Fontaine, F. Gucci, V. Dorcet, T.G. Saunders, M. Yu, F. Cheviré, C. Boussard-Pledel, J.-F. Halet, R. Gautier, M.J. Reece, B. Bureau, Effect of the Processing Route on the Thermoelectric Performance of Nanostructured $\text{CuPb}_{18}\text{SbTe}_{20}$, *Inorg. Chem.* 57 (2018) 12976–12986. doi:10.1021/acs.inorgchem.8b02248.
- [28] B. Srinivasan, C. Boussard-Pledel, B. Bureau, Thermoelectric performance of codoped (Bi, In)-GeTe and (Ag, In, Sb)-SnTe materials processed by Spark Plasma Sintering, *Mater. Lett.* 230 (2018) 191–194. doi:10.1016/j.matlet.2018.07.132.
- [29] B. Srinivasan, A. Gellé, F. Gucci, C. Boussard-Pledel, B. Fontaine, R. Gautier, J.-F. Halet, M.J. Reece, B. Bureau, Realizing a stable high thermoelectric $zT \sim 2$ over a broad temperature range in $\text{Ge}_{1-x-y}\text{Ga}_x\text{Sb}_y\text{Te}$ via band engineering and hybrid flash-SPS processing, *Inorg. Chem. Front.* 6 (2019) 63–73. doi:10.1039/C8QI00703A.
- [30] M. Sato, T. Kamimura, T. Iwata, Magnetic properties and anisotropy of $(\text{Fe}_{1-x}\text{Co}_x)_7\text{Se}_8$, *J. Appl. Phys.* 57 (1985) 3244–3246. doi:10.1063/1.335112.
- [31] E. Zuñiga-Puelles, R. Cardoso-Gil, M. Bobnar, I. Veremchuk, C. Himcinschi, C. Hennig, J. Kortus, G. Heide, R. Gumeniuk, Structural stability and thermoelectric performance of high quality synthetic and natural pyrites (FeS_2), *Dalton Trans.* 48 (2019) 10703–10713. doi:10.1039/C9DT01902B.
- [32] M. Shirai, N. Suzuki, K. Motizuki, Electronic band structure and photoemission spectra of Fe_7S_8 , *J. Electron Spectrosc. Relat. Phenom.* 78 (1996) 95–98. doi:10.1016/S0368-2048(96)80035-1.

Pre-print Version